Petroleum Science 19 (2022) 387–396

Contents lists available at ScienceDirect

Petroleum Science

journal homepage: www.keaipublishing.com/en/journals/petroleum-science

Original Paper

Plugging property and displacement characters of a novel high-temperature resistant polymer nanoparticle

Zhi-Yong Wang [a, b, *], Mei-Qin Lin [a, **], Huai-Ke Li [b], Zhao-Xia Dong [c, ***], Juan Zhang [a], Zi-Hao Yang [a]

[a] Unconventional Petroleum Research Institute, China University of Petroleum (Beijing), Beijing, 102249, People's Republic of China
[b] Oilfield Chemicals R&D Institute, China Oilfield Services Limited, Langfang, 065201, People's Republic of China
[c] China University of Geosciences (Beijing), Beijing, 100083, People's Republic of China

ARTICLE INFO

Article history:
Received 3 December 2020
Accepted 5 March 2021
Available online 3 November 2021

Edited by Xiu-Qiu Peng

Keywords:
Polymer nanoparticles
High temperature resistance
Plugging property
EOR

ABSTRACT

The goal of the research was to investigate the profile control and oil displacement characteristics of the polymer nanoparticles after high temperature swelling. The displacement parameters showed considerable influence on the plugging effect of the high-temperature swelled polymer nanoparticles, such as the core permeability, concentration of nanoparticles in the suspension, swelling time and swelling temperature, which makes it flexible to control the plugging effect by controlling displacement experiments conditions. Experimental results show that polymer nanoparticles dispersion system with a concentration of 500 mg/L is suitable for cores plugging with a permeability of 30×10^{-3} - 150×10^{-3} μm^2, even after aging at 150 °C for three months. The shunt flow experiments show that when the displacement factors are optimal values, the polymer nanoparticles after high temperature swelling to plug the high-permeability layer selectivity and almost do not clog the low-permeability layer. Oil recovery of homogeneous artificial core displacement experiment and a heterogeneous double-tube cores model are increased by 20% and 10.4% on the basis of water flooding. The polymer nanoparticles can be a great help for petroleum engineers to better apply this deep profile control and flooding technology.

1. Introduction

Water flooding is one of the most important methods in the development of oilfield, water-out inevitably appear in high permeability layer after water flooding development, which can result in the sweep efficiency decrease of injected water (You et al., 2019; Feng et al., 2019; Ebrahim et al., 2019). Conformance control treatment can plug the high permeability layer, increase the sweep efficiency of injected water and improve the oil recovery (Zhu et al., 2017, 2018; Zhao et al., 2018, 2019; Kang et al., 2019). The frequently-used conformance control materials are colloidal dispersion gels (Abdulbaki et al., 2014; BjoRsvik et al., 2008), weak gel (Pu et al., 2017; Chen et al., 2018; Wang et al., 2017; Omari et al., 2006; Hasankhani et al., 2019; Lashari et al., 2018), preformed particle gel (Sang et al., 2014; Lenji et al., 2018; Pu et al., 2018a,b) and polymer microspheres (Yao et al., 2015; Yang et al. 2015, 2017; Lin et al., 2015; Pu et al., 2018a,b). Polymer microsphere conformance control technology is a new deep conformance control technology in recent years. The particle size of polymer microspheres used in the oilfield is from nanoscale to micron scale and the particle size is controllable (Ye et al., 2002; Wang et al., 2019). Polymer microsphere is not difficult to disperse in water and form a dispersion system (Jiang et al., 2015). Polymer microsphere has the water swelling property because of its spatial network structure (Wang et al., 2018; Zhao et al., 2014). In addition, polymer microsphere does not increase the viscosity of the injection system, therefore, will not increase the resistance of the injection pipeline. Polymer microsphere has strong temperature and salt tolerance and good adaptability. Polymer microsphere has not only conformance control effect, but also oil displacement effect (Inomata

* Corresponding author.
** Corresponding author.
*** Corresponding author.
E-mail addresses: zoyicup@126.com (Z.-Y. Wang), 13910509321@163.com (M.-Q. Lin), dzx@cup.edu.cn (Z.-X. Dong).

https://doi.org/10.1016/j.petsci.2021.08.010

et al., 1995).

Polymer microspheres are often used with polymers in the oilfield. The commonly used polymer is partially hydrolyzed polyacrylamide (HPAM) (Wang et al. 2018, 2019). The high temperature resistance of acrylamide microspheres is very poor. Many researchers improve the high temperature resistance performance by adding functional monomers, such as 2-acrylamide group-2-methyl propyl sulfonic acid (AMPS), 1-vinyl-2-pyrrolidinon (NVP), N, N-Dimethyl acrylamide (DMAM), etc. However, they cannot be accord with requirements of high temperature and high salinity reservoirs (Liu et al., 2014; Gao et al. 2011; Lin et al., 2020).

In our previous work, Zr-induced thermostable polymeric nanospheres with double-*cross*-linked architectures were prepared through inverse emulsion copolymerization (Wang et al., 2019). In this work, a total of 20 core flood tests were carried out to investigate the displacement characters of this flooding system, including the core permeability, concentration of nanoparticles, swelling time and swelling temperature, and the displacement efficiency of the system in homogeneous and heterogeneous cores was also investigated. The basic parameters of the cores are shown in Table 1.

2. Materials and methods

2.1. Materials

Main composition sodium chloride (NaCl, AR), magnesium chloride ($MgCl_2$, AR), potassium chloride (KCl, AR), calcium chloride ($CaCl_2$, AR), sodium carbonate (Na_2CO_3, AR), sodium bicarbonate ($NaHCO_3$, AR), methylene blue (dye content, ≥90%) and. All the above materials were purchased from Shanghai Macklin Biochemical Co. LTD, China. All of the above substances were used without any further purification. Artificial cores provided by China University of Petroleum, Beijing.

2.2. Optical microscopic observation

A drop of swelled nanoparticle solution was placed onto the surface of a clean glass slide, which was stained with methylene blue solution for observation under an Olympus BX41 microscope manufactured by the Olympus Company (Japan).

Table 1
Physical parameters of cores.

core no.	L, mm	D, mm	PV, mL	φ, %	K_w, ($\times 10^3 \mu m^2$)
1#	151	25.0	20.8	28.07	30.04
2#	150	25.1	21.6	29.83	90.63
3#	150	25.2	22.2	29.93	156.18
4#	149	24.9	23.5	32.15	225.47
5#	151	25.0	24.7	33.61	304.21
6#	151	25.2	20.7	27.94	89.21
7#	149	25.1	20.8	28.69	90.06
8#	150	25.0	20.5	27.64	89.14
9#	151	25.3	20.7	27.94	89.69
10#	149	25.1	20.8	28.69	90.12
11#	150	25.0	20.5	27.64	89.19
12#	148	25.1	20.7	27.83	89.24
13#	150	24.9	20.6	27.77	88.93
14#	149	25.0	20.4	27.91	89.18
15#	152	25.1	20.3	27.88	89.15
16#	151	25.2	20.5	27.89	90.11
17#	150	24.9	20.5	27.64	88.48
18#	149	25.1	20.8	28.69	91.27
19#	150	25.0	20.6	27.77	89.36
20#	151	25.0	20.7	27.94	88.95

2.3. Long term high-temperature resistance

About 0.2 g of polymer nanoparticles was placed in an ampoule bottle containing 40 ml brine, then the ampoule bottle was placed under vacuum and sealed. Finally, the sample was placed in a constant temperature environment (150 °C), and then the swelling phenomenon was observed by an optical microscope, along with the measurement of the particle size distribution by a laser particle sizer. When the polymer nanoparticles were almost completely degraded, the process of temperature resistance was considered finished.

2.4. Experiment of plugging performance

First, measure the length L, width D and height H of the square core, put the core in a drying oven at 100 °C for 5 h, and then weigh the dry weight W_1 on the electronic balance. In the vacuum pumping device, the core is vacuumized for 8 h, then saturated with brine for 8 h, and weighed the wet weight mass W_2. and the porosity of core matrix void volume PV Φ is calculated.

2.5. Experiment of enhanced oil recovery (EOR)

Re dried core was inserted into the core holder, and vacuumized for more than 6h at 65 °C. Salt water (2 PV, salinity of 5000 mg/L) was injected into the artificial core at a stable flow rate of 0.40 mL/min until the monitored pressure tended to be stable, then, the simulated oil was injected at the pump speed of 0.4 mL/min, and samples are collected at the outlet end of tubes with different specifications. The water content and water content of each tube are measured, and the water content is calculated. Until the water content in the tube reaches below 2%, the sum of the volumes of water in all tubes is the volume of saturated simulated oil. Therefore, the cores were all saturated by the simulated oil sample and the crude oil saturations (S_{coi}, %) and initial oil volume (V_{oi}, mL) were calculated. Subsequently, Water drive the core with an injection flow rate of 0.4 mL/min, at the same time, the test tubes of different specifications are used to collect samples and monitor the pressure change at the outlet of the core. The liquid content and oil content in the test tubes were measured at the right time, and the oil content and water content are calculated until the water content in the test tubes reaches more than 98%, and the residual oil volume (V_{re}, mL) was calculated. At the same flow rate, the 4.0 PV nanoparticles solution swelled at 150 °C for 90 days was injected. The samples were collected at the right time and contents of the oil and water were calculated. At the end of the solution injection, salt water was injected until the water content in the test tube reached more than 98%. Finally, the oil increment volume (ΔV, mL) was recorded and the oil recovery of brine water flooding (R_w, %) and enhanced oil recovery of the high-temperature swelled nanoparticles (EOR, %) was calculated using eqs (1) and (2). The resistance coefficient (RC) and residual resistance coefficient (RRC) are calculated by equations (3) and (4) respectively.

$$R_w(\%) = \frac{V_{oi} - V_{re}}{V_{oi}} \times 100\% \quad (1)$$

$$EOR(\%) = \frac{\Delta V}{V_{oi}} \times 100\% \quad (2)$$

$$RC = \frac{(\Delta P)_{SP}}{(\Delta P)_{wb}} \quad (3)$$

$$RCC = \frac{(\Delta P)_{wa}}{(\Delta P)_{wb}} \quad (4)$$

Where $(\Delta P)_{SP}$ is the stable pressure drop at both ends of core during polymer nanoparticle injection (profile control process), $(\Delta P)_{wb}$ the stable pressure drop at both ends of core during water injection before profile control, $(\Delta P)_{wa}$ the stable pressure drop at both ends of core during water injection after profile control.

3. Results

3.1. Long term high-temperature resistance

Fig. 1 are the micrographs of nanoparticles at different swelling times at 150 °C. Obviously, the particle size of polymer nanoparticles gradually increases with the increase of swelling time. A smooth surface and a perfect spherical shape (Fig. 1b–e) were observed in the polymer nanoparticles after swelling for different days at 150 °C. Dark spots appeared in the center of the particle after 170 days (Fig. 1h). However, the structure of the polymer nanoparticles obviously changed when the swelling time reached 180 days. As shown in Fig. 1i, a structure of spines appeared in the polymer nanoparticles. So far, it was difficult to explain the phenomenon of the resulting polymer nanoparticles within the structure of spines. However, it is very likely that poly-nuclear olation complex ions were formed between the hydrolyzed metal crosslinking agent. With the hydrolysis of the polyacrylamide molecular chain, the structure of the acrylic acid and the poly-nuclear olation complex ions formed a more compact network structure by a coordination substitution reaction. Finally, a dense three-dimensional network structure filled the interior of the polymer nanoparticles.

3.2. Effect of permeability to plugging property

As shown in Fig. 2, the injection pressure change in single core models with different permeability (I, primary water injection; II, injection of high-temperature swelled nanoparticles solution; and III, succeeding water injection). It can be seen that when injecting the nanoparticles dispersion system of 4 PV, with the increase of core permeability, the pressure at the core inlet decreases gradually, which are 2372.3 kPa, 523.6 kPa, 242.9 kPa, 77.5 kPa and 29.4 kPa respectively. This shows that the high-temperature swelled nanoparticles dispersion system has a good plugging effect for the cores with small permeability (30×10^{-3}-150×10^{-3} μm^2, Fig. 2 a-c), but a poor sealing effect for the cores with large permeability (225×10^{-3}-305×10^{-3} μm^2, Fig. 2 d-e). Obviously, the maximum pressure in the middle section of the core with a permeability of 30×10^{-3} μm^2 is 108.14 kPa (Fig. 2a), which is far lower than the pressure value of 2372.33 kPa at the inlet. It can be seen that the deep migration performance of the high-temperature swelled nanoparticles in the core with a permeability of 30×10^{-3} μm^2 is poor. For core pore structure, the size of high-temperature swelled nanoparticles after 30 days is large enough, so they can only stay at the entrance of the core. In Fig. 2b and c, the middle sections of core with permeability of 90×10^{-3} μm^2 and 150×10^{-3} μm^2 have higher pressure values, which are 178.09 kPa and 88.24 kPa respectively. This shows that high-temperature swelled nanoparticles have good plugging effect and deep migration ability in the cores with permeability of 90×10^{-3} μm^2-150×10^{-3}. The pressures at the core inlet with

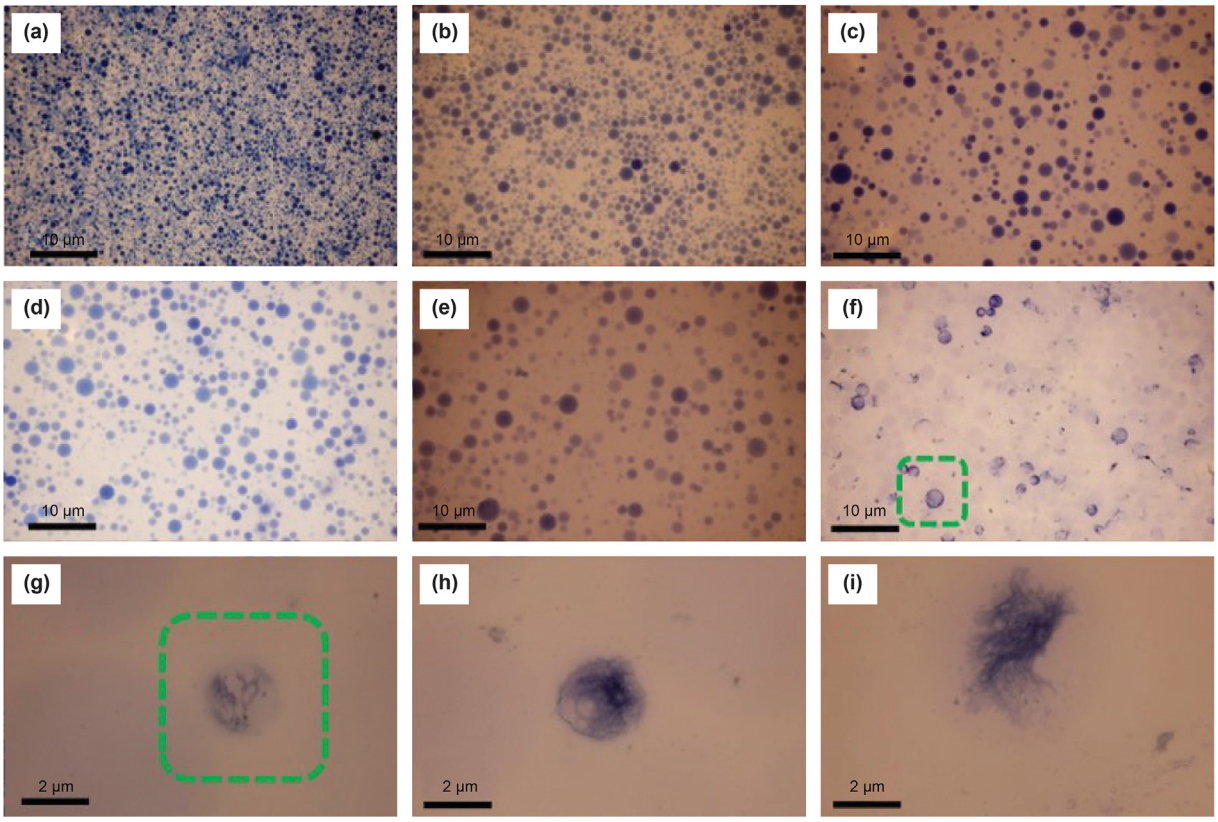

Fig. 1. Micrograph of nanoparticles at different swelling times at 150 °C (a-2 day; b-10 days; c-30 days; d-80 days; e–120 days; f-150 days; g-partial enlargement of (f); h-170 days; i-180 days.).

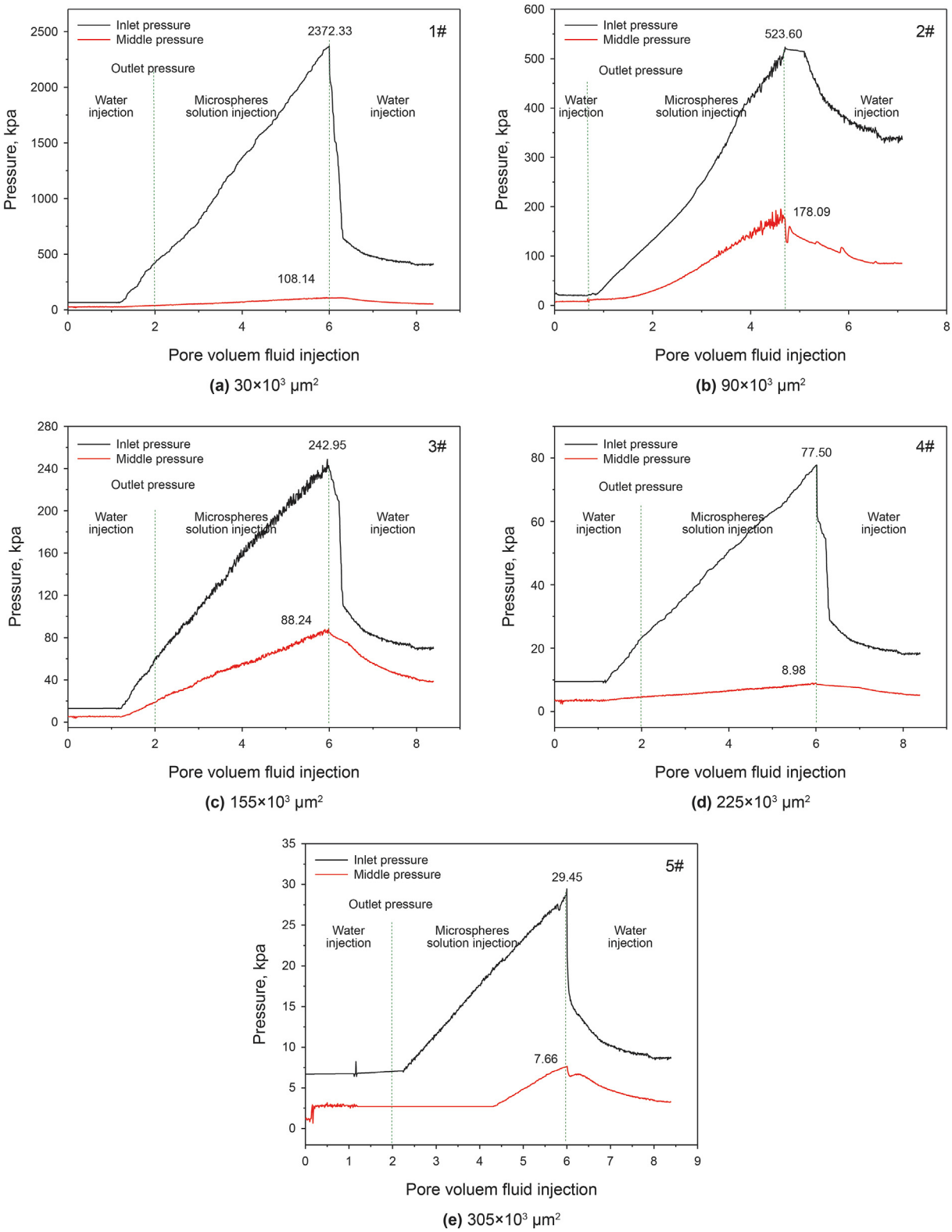

Fig. 2. Injection pressure change in single-tube sand pack models with different permeability (salinity: 10000 mg/L; concentration of nanoparticles: 500 mg/L; swelling time: 30 days; swelling temperature: 150 °C; injection rate: 0.4 mL/min).

permeability of 225 × 10^{-3} μm² and 305 × 10^{-3} μm² are 77.50 kPa and 29.45 kPa, the middle pressures are 8.98 kPa and 7.66 kPa respectively from the pressure curves of Fig. 2d and e. The above experimental results show that the swelled nanoparticles dispersion system swelled 30 days at 150 °C is suitable for plugging core with a permeability of 90 × 10^{-3}-150 × 10^{-3} μm². At the same time,

the swelled nanoparticles can enter the deep part of the core and play a role of deep profile control. It also indirectly shows that nanoparticles have excellent high temperature resistance.

3.3. Effect of concentration to plugging property

The concentration of high-temperature swelled nanoparticles dispersion system will not only affect its plugging effect on porous media, but also affect its in-depth migration effect. The injection pressure change in single core models with different permeability (I, primary water injection; II, injection of high-temperature swelled nanoparticles solution; and III, succeeding water injection) as shown in Fig. 3. When the mass concentration of the high-temperature swelled nanoparticles dispersion system is 200 mg/L, pressure of the core inlet is 197.09 kPa, and the middle pressure is 48.21 kPa after injecting the 4 PV this dispersion system. This dispersion system (200 mg/L) has a certain plugging effect on the core with a permeability of 90×10^{-3} μm^2, and some nanoparticles can also migrate to the middle of the core. However, both the pressure at the core inlet and the pressure at the middle section decreased significantly after succeeding water injection, which are maintained at about 90 kPa and 15 kPa respectively. The coefficient of residual resistance is small, which is 5.06 and 1.76 respectively, indicating that the nanoparticles dispersion system with this concentration has poor plugging effect on the core. When the mass concentration of the dispersion system is 500 mg/L, the pressure at the core inlet is 523.60 kPa, the pressure at the core middle section is 178.09 kPa, and the resistance coefficient is 26.18 and 22.26, respectively. Both the pressure at the core inlet and the pressure at the middle section decreased significantly after succeeding water injection, which are maintained at about 340 kPa and 85 kPa respectively. The coefficient of residual resistance is small, which is 5.06 and 1.76 respectively, the coefficient of residual resistance is 17.42 and 10.73, respectively. It can be seen that the nanoparticles dispersion system of this concentration has a good plugging effect on the core with a permeability of 90×10^{-3} μm^2, and most nanoparticles can also migrate to the middle part of core. The pressure at the core inlet is 1209.56 kPa, and the pressure at the middle part of the core is 62.59 kPa after injection of 4 PV microsphere dispersion system (1000 mg/L), indicating that the nanoparticles is almost blocked at the core inlet and can't move forward and deeply, so it does not reach the back part of the core. This is mainly because the concentration of the swelled nanoparticles dispersion system is too large, which is easy to form aggregation and bridging in the pore channel of the core port and block it, resulting in that the injected microsphere can not move forward, and the compression and accumulation between the swelled nanoparticles makes the pressure at the inlet rapidly rise, while the pressure value of the rock core segment is low due to the limited number of swelled nanoparticles moving here. The results show that the nanoparticles with 30 days swelled at 150 °C can effectively block the core with a permeability of 90×10^{-3} μm^2, and the optimal mass concentration of the nanoparticles with good migration performance is 500 mg/L.

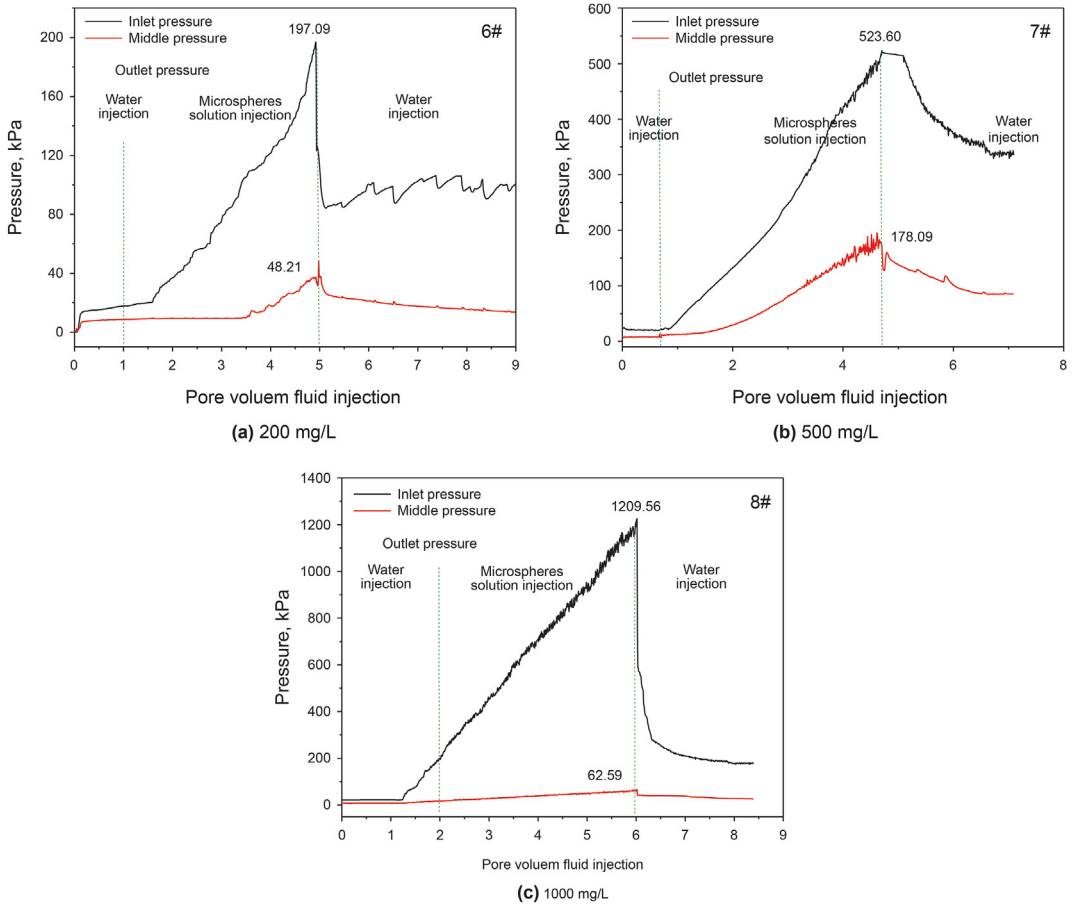

Fig. 3. Injection pressure change in single-tube sand pack models with different concentration (salinity: 10000 mg/L; core permeability: 90×10^{-3} μm^2; swelling time: 30 days; swelling temperature: 150 °C; injection rate: 0.4 mL/min).

3.4. Effect of swelling time to plugging property

The size of the nanoparticles is different under different swelling time, so the elasticity and toughness are different, which will have a certain impact on the plugging effect and the migration in the core. The injection pressure change in single core models with different swelling time (I, primary water injection; II, injection of high-temperature swelled nanoparticles solution; and III, succeeding water injection) as shown in Fig. 4. It can be seen from Fig. 4 that when the nanoparticles dispersion system (same concentration and the same number of PV) are injected into the cores, with the increase of the swelling time, the pressure at the core inlet and at the middle section both increase first and then decrease. Fig. 4 a shows that the un-swelling nanoparticles have weak plugging effect on the core and strong migration ability, because the dry powder nanoparticles are almost a solid rigid sphere with small particle size and no elasticity. The pressure at the core inlet increases rapidly from 43.92 kPa to 169.02 kPa, the pressure at the middle section increases from 16.10 kPa to 42.80 kPa when the nanoparticles swelled for 3 days. Meanwhile, the swelling time of the nanoparticles continues to increase to 5 days, 10 days, 20 days and 30 days. Both the pressure at the core inlet and the pressure at the middle section continue to increase. It is thus clear that during this period of time, the nanoparticles gradually swell, water molecules slowly enter the interior of the nanoparticles, the originally twisted and folded molecular chains slowly expand under the action of repulsion force and the size of nanoparticles increases gradually. Therefore, the plugging effect of the core with the same permeability is getting better and better. At the same time, because the molecular chain is not fully extended and the nanoparticles are not fully expanded, the result is that nanoparticles exhibit good elasticity and mobility. When the swelling time is 60 days, the pressure at the core inlet is 407.99 kPa, and the pressure at the middle section is 110.60 kPa. At this time, the resistance coefficients at the inlet and middle section are 16.32 and 9.22, the residual resistance coefficients after the succeeding water injection are 9.84 and 3.67, respectively. The pressure values at the core inlet and middle sections are reduced to 248.09 kPa and 92.99 kPa, continuing to extend the swelling time for 90 days. Meanwhile, the resistance coefficients at the inlet and middle section are 9.97 and 7.75, the residual resistance coefficients after the succeeding water injection are 7.52 and 2.68, respectively. Obviously, the nanoparticles with high temperature swelling for 60 days show better plugging and migration performance. Fortunately, the nanoparticles swelled at high temperature for 90 days also partly had plugging and migration performance. Quite evidently, this indirectly shows that nanoparticles have excellent high temperature resistance.

3.5. Effect of swelling temperature to plugging property

In the same swelling time, the swelling temperature directly affects the properties of polymer nanoparticles. Such as the size and elasticity of nanoparticles so on. The injection pressure change in single core models with different swelling temperature (I, primary water injection; II, injection of high-temperature swelled nanoparticles solution; and III, succeeding water injection) as shown in Fig. 5. It can be seen from Fig. 5 that when the nanoparticles dispersion system (same concentration of 500 mg/L and the same number of 4 PV) are injected into the cores, with the increase of the swelling temperature, the maximum pressure values at the core inlet are 443.62 kPa, 523.60 kPa, 565.34 kPa and 580.27 kPa. It can be seen that the higher the swelling temperature at the same swelling time, the faster the swelling rate of the microsphere, and the larger the diameter of the microsphere, the better the sealing effect of the core. As the swelling temperature increases, the pressure values in the middle section of the core are 122.19 kPa, 178.09 kPa, 186.27 kPa and 136.73 kPa, respectively, showing a trend of first increasing and then decreasing. The results show that the higher the swelling temperature, the faster the swelling rate. Therefore, polymer nanoparticles the small particle size at 100 °C have a certain sealing effect on the core and can also migrate to the middle and back sections of the core. However, after the succeeding water injection, the pressure at the inlet and middle sections of the core dropped to 310 kPa and 65 kPa, and the residual resistance coefficients are relatively small, 12.41 and 5.42, respectively. Because of swelling at 100 °C for 30 days, the microspheres are still in the early stage of swelling, with small particle size and weak elasticity. Therefore, when the swelling temperature is 100 °C, the emulsion polymer nanoparticle need longer swelling time (>30 days) to show better sealing and migration performance. When the swelling temperature is 120 °C and 140 °C, the resistance coefficient in the middle section of the core after injection of the 4Vp polymer nanoparticles dispersion system is 14.84 and 15.52, respectively. The pressure drops little after the succeeding water injection, and the residual resistance coefficient in the middle section of the core is 8.33 and 10.24, respectively. The polymer nanoparticles show good sealing and migration performance. Because the polymer nanoparticles are in the middle stage of swelling at 120 °C and 140 °C for 30 days, with moderate particle size and good elasticity, this nanoparticles swelling for 30 days at 120 °C and 140 °C can meet the blocking and migration demand of regulating flooding. When the swelling temperature was 150 °C, the resistance coefficients at the entrance and middle of the core are 25.23 and 11.39, respectively, and the residual resistance coefficients after the succeeding water injection are 18.48 and 4.93, respectively. It can be seen that polymer nanoparticles swelling for 30 days at 150 °C also had good sealing and migration performance.

3.6. Effect of enhanced oil recovery

3.6.1. Homogeneous cylindrical core

Core displacement experiment was used to evaluate the effect of polymer nanoparticles dispersion system on EOR of homogeneous cores. The effect of enhanced oil recovery of polymer nanoparticles dispersion system with a mass concentration of 500 mg/L was investigated at the core containing oil with permeability of 90×10^{-3} μm^2. Fig. 8 show the change in cumulative oil recovery, water cut, and pressure history with displaced fluid at a fixed salt concentration of 10000 mg/L (Na^+: 2396 mg/L, K^+: 747.5 mg/L, Mg^{2+}: 289 mg/L, Ca^{2+}: 309 mg/L, Cl^-: 5117.5 mg/L, HCO_3^-: 1141 mg/L). From Fig. 6, it can be seen that the oil recovery increased with the increase of water injection volume, the core pressure value increased rapidly by injecting 4 PV high-temperature swelled nanoparticles dispersion system, the maximum pressure value is 525.19 kPa, the water content decreases, the oil recovery increased sufficiently 13% from 29% to 42%. Fortunately, the pressure value decreased only about 345 kPa and the oil recovery increased to 50% after chase water flooding.

The injectivity and plugging performance of the high-temperature swelled nanoparticles were evaluated by resistance factor (RF) and residual resistance factor (RRF). The increase of 510 kPa in differential pressure during the injection period of nanoparticles dispersion system at 150 °C indicated that high-temperature swelled nanoparticles had fine injectivity and were capable of penetrating deeply into the petroleum formation. Before injection, the nano-polymer particles were swelled to certain extent, therefore their particle sizes have no big change after injection since the temperature remains unchanged. After the homogeneous cylindrical core was treated by high-temperature

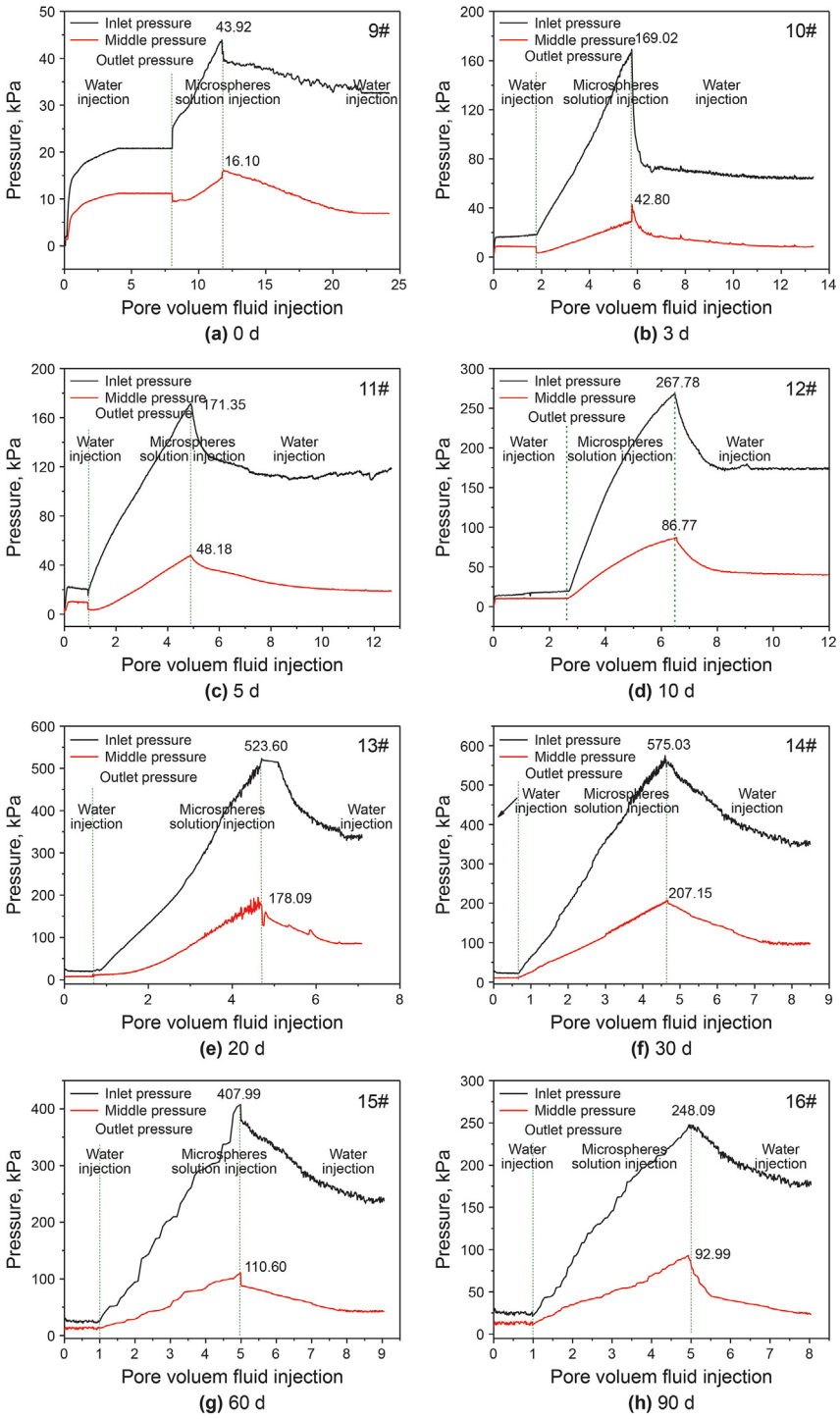

Fig. 4. Injection pressure change in single-tube sand pack models with different swelling time (salinity: 10000 mg/L; core permeability: 90 × 10^{-3} μm^2; concentration of nanoparticles: 500 mg/L; swelling temperature: 150 °C; injection rate: 0.4 mL/min).

swelled nanoparticles dispersion system at 150 °C for 3 months, and during chase water flooding, the differential pressure was decreased to 425 kPa. It could be calculated that the residual resistance factor was 10.63 and the plugging efficiency was 93.9%, indicating that the high-temperature swelled nanoparticles have excellent resistance to high temperature and plugging performance. After aging at 150 °C, the nano-polymer particles's particle size gradually increased on account of its excellent thermal stability under high temperature, thus blocking pores and throat channels through adsorption, retention, deformation and other mechanisms (Liu et al., 2012).

3.6.2. Heterogeneous cylindrical core

A heterogeneous double-tube sand pack model was used in this study to study the profile control and displacement performance of nano-polymer particles dispersion system. A 500 mg/L nano-

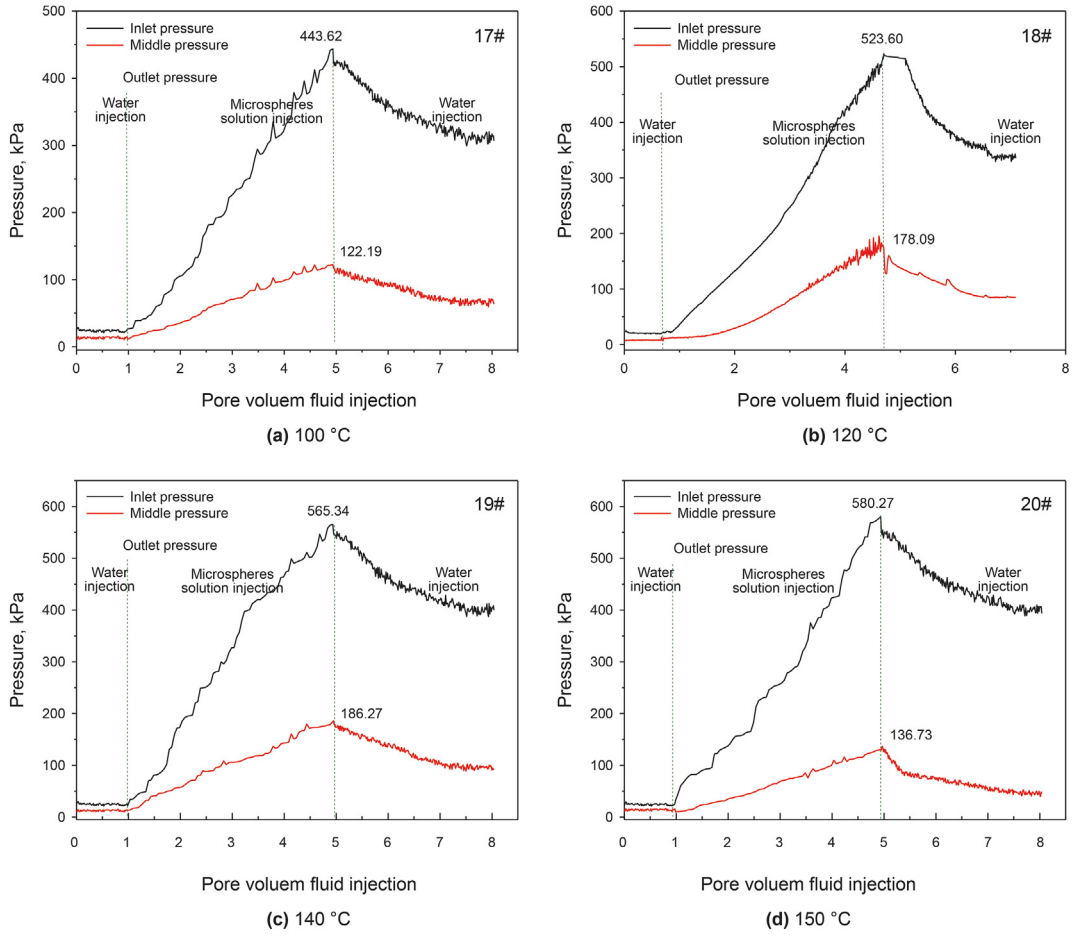

Fig. 5. The effect of swelling temperature on plugging and migration characteristics of polymer nanoparticle (salinity: 10000 mg/L; core permeability: 90 × 10^{-3} μm^2; concentration of microspheres: 500 mg/L; swelling time: 30 d; injection rate: 0.4 mL/min).

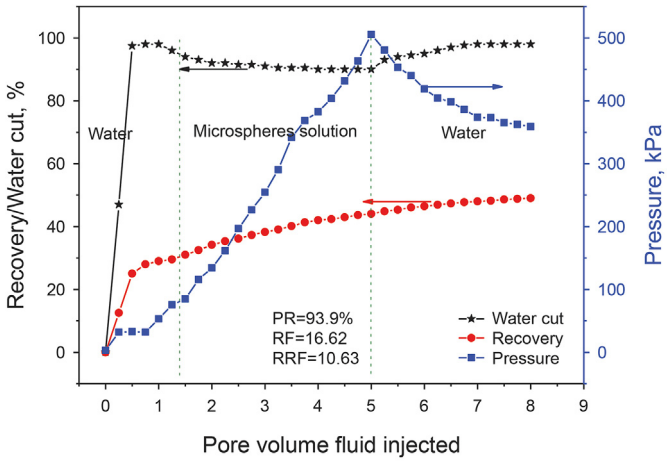

Fig. 6. Cumulative oil recovery, water cut, and pressure history of different pore volume fluid injected (concentration of the microsphere: 500 mg/L; swelling time: 30 days; swelling: temperature: 150 °C).

polymer particles dispersion system was prepared with simulated salt water with a salinity of 10000 mg/L and swelled at 150 °C for 30 days. The slug size of the injected microsphere dispersion system was 4 PV. The experimental results are shown in Table 2, Figs. 7 and 8.

It can be seen from the data in Table 2 that in the early stage of water drive of parallel double pipe model, the recovery of high permeability tube is about 27.2%, while that of low permeability tube is only 17.6%, which is about 10% lower than that of high permeability tube. This shows that in the early stage of injection of simulated salt water, the simulated salt water mainly passes through the high-permeability core with low flow resistance, and part of it passes through the low-permeability core with high flow resistance, so that the recovery of high-permeability core is significantly higher than that of low-permeability core. As shown in Fig. 7, the pressure value rises rapidly with the maximum value of 929.64 kPa after injection of microsphere dispersion system slug, and the pressure value gradually decreases after chase water flooding. The final total recovery of double pipe is 33.2%, in which the recovery of low-permeability pipe is 29.8%, and that of high-permeability pipe is 35.4%. The difference between the two is small. However, from the data in Table 2, it is found that the recovery of microsphere dispersion system in low-permeability pipe is 12.2%, while that in high-permeability tube is only 8.2%, which is 4.0% lower than that in low-permeability tube, and the recovery of double tube core is 10.4% higher on the basis of water drive. It can be seen that the injected nano-polymer particles dispersion system preferentially enters the high-permeability core and blocks the large pore in the high-permeability core. Because the microsphere dispersion system has the effect of plugging and profile control, when the double tube model is used for water drive, the injected water enters the low-permeability core and displaces the

Table 2
Physical parameters of cores and nano-polymer particles dispersion system double-tube displacement results.

Core Permeability, $\times 10^{-3}$ μm^2	S_{oi}, %	R_w, %		R_{N-P}, %		EOR, %	
		single	total	single	total	single	total
30	75.2	17.6	22.8	12.2	10.4	29.8	33.2
90	73.9	27.2		8.2		35.4	

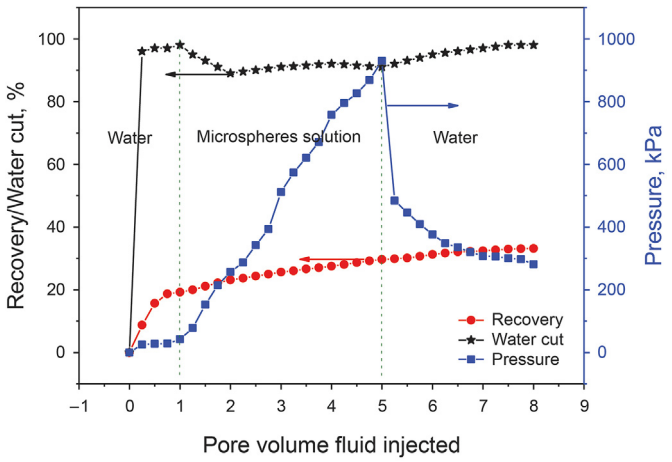

Fig. 7. Double-tube flooding experiment recovery, water content and the relationship between injection volume (concentration of the microsphere: 500 mg/L; swelling time: 30 days; swelling temperature: 150 °C).

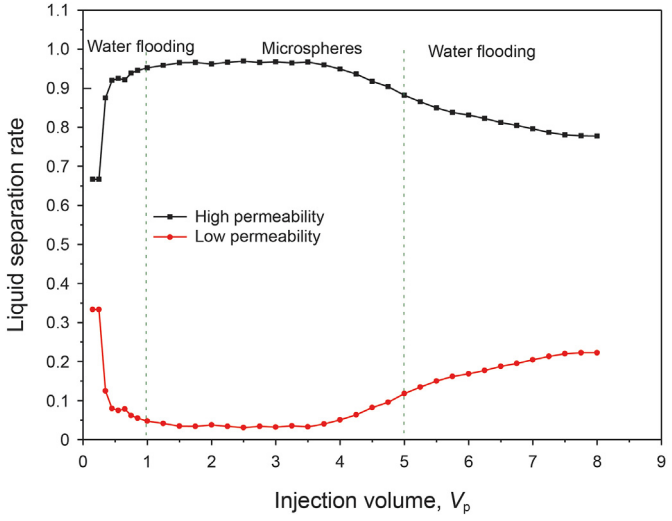

Fig. 8. Double-tube experiments in parallel watershed between rate and injection volume (concentration of the microsphere: 500 mg/L; swelling time: 30 days; swelling temperature: 150 °C).

remaining oil or residual oil zone that the first water drive did not affect. Therefore, the pressure in the model increases obviously and the water content of the produced liquid decreases after the injection of the microsphere dispersion system.

Fig. 8 is the relationship curve between the liquid separation rate and injection volume of parallel double tubes displacement. It can be seen from the Figure that as the injection slug of the nano-polymer particles dispersion system increases, the liquid separation rate of the low-permeability core increases, and the liquid separation rate of the high-permeability core decreases, which also shows that the injection of the nano-polymer particles dispersion system has played a sealing role in the high-permeability core, achieving a better liquid flow steering effect, making the subsequent displacement fluid enter the low-permeability core, starting the residual oil in it, and achieving the purpose of EOR. It can be seen that nano-polymer particles dispersion system has certain plugging and displacement control effect on high permeability core when swelling for 30 days at 150 °C.

4. Conclusions

In this paper, the polymer nanoparticles dispersion system with a concentration of 500 mg/L could exhibit an effective plugging effect for cores with different permeability from 30 $\times$ 10^{-3} μm^2 to 150 $\times$ 10^{-3} μm^2, even after aging at 150 °C for 90 days. The polymer nanoparticles dispersion system after high temperature swelling has a good effect on the control and displacement of homogeneous core, and the oil recovery is improved by 20% on the basis of water drive. This system could significantly reduce fractional flow through high permeability channel, and also present good profile control effect and oil displacement efficiency in parallel double cores, and the recovery of double tube core is increased by 10.4% on the basis of water drive. Obviously, this work provides a kind of new material to meet the demand of tertiary oil recovery in high temperature reservoirs. The novel high-temperature resistant polymer nanoparticle can be a great help for petroleum engineers to better apply this deep profile control and flooding technology.

Acknowledgements

This research was funded by National Natural Science Foundation of China No. 51874316 and 51274211 and National Key Scientific and Technological Project (Grant No. 2017ZX05009-004).

References

Abdulbaki, M, Huh, C, Sepehrnoori, K, Delshad, M, Varavei, A, 2014. A critical review on use of polymer microgels for conformance control purposes. J. Petrol. Sci. Eng. 122, 741–753. https://doi.org/10.1016/j.petrol.2014.06.034.

BjoRsvik, M, Holland, H, Skauge, A, 2008. Formation of colloidal dispersion gels from aqueous polyacrylamide solutions. Colloids Surf. A Physicochem. Eng. Asp. 317, 504–511. https://doi.org/10.1016/j.colsurfa.2007.11.025.

Chen, LF, Wang, JJ, Yu, L, Zhang, Q, Fu, ML, et al., 2018. Experimental investigation on the nanosilica-reinforcing polyacrylamide/polyethylenimine hydrogel for water shutoff treatment. Energy Fuels 32, 6650–6656. https://doi.org/10.1021/acs.energyfuels.8b00840.

Ebrahim, T, Mohsen, VS, Mahdi, SM, Mahdi, SM, Esmaeel, KT, Saeb, A, 2019. Performance of low-salinity water flooding for enhanced oil recovery improved by SiO_2 nanoparticles. Petrol. Sci. 16, 131–139. https://doi.org/10.1007/s12182-018-0295-1.

Feng, Q, Liu, H, Peng, ZG, Zheng, Y, 2019. Preparation of a cationic hyperbranched polymer for inhibiting clay hydration swelling in the process of oilfield waterflooding. Energy Fuels 33, 12202–12212. https://doi.org/10.1021/acs.energyfuels.9b02777.

Gao, L, Sun, DJ, Xu, J, 2011. Preparation and properties of P(AMPS-AM-DMAM-NVP) as fluid loss reducer. Polym. Mater. Sci. Eng. 41, 675–679. https://doi.org/10.1016/S0040-4039(99)02163-2 (In Chinese).

Hasankhani, GM, Madani, M, Esmaeilzadeh, F, Mowal, D, 2019. Experimental investigation of asphaltene-augmented gel polymer performance for water shut-off and enhancing oil recovery in fractured oil reservoirs. J. Mol. Liq. 275, 654–666. https://doi.org/10.1016/j.molliq.2018.11.012.

Inomata, H, Wada, N, Yagi, Y, Goto, S, Saito, S, 1995. Swelling behaviours of N-alkylacrylamide gels in water: effects of copolymerization and crosslinking density. Polymer 36, 875–877. https://doi.org/10.1016/0032-3861(95)93120-B.

Jiang, JF, Zhao, Q, Lin, MQ, Wang, YF, Dang, SM, Sun, FF, 2015. A study of factors affecting properties of AM/AMPS/NVP terpolymeric microspheres prepared by inverse suspension polymerization. Iop. Confer. 103, 012046. https://doi.org/10.1088/1757-899X/103/1/012046.

Kang, WL, Cao, CX, Guo, SJ, Tang, XC, Lashari, ZA, Gao, YB, et al., 2019. Mechanism of silica nanoparticles' better-thickening effect on amphiphilic polymers in high salinity condition. J. Mol. Liq. 277, 254–260. https://doi.org/10.1016/j.molliq.2018.12.092.

Lashari, ZA, Yang, HB, Zhu, Z, Tang, XC, Cao, CX, Iqbal, MW, Kang, WL, 2018. Experimental research of high strength thermally stable organic composite polymer gel. J. Mol. Liq. 263, 118–124. https://doi.org/10.1016/j.molliq.2018.04.146.

Lenji, MA, Haghshenasfard, M, Sefti, MV, Salehi, MB, Heidari, A, 2018. Experimental study of swelling and rheological behavior of preformed particle gel used in water shutoff treatment. J. Petrol. Sci. Eng. 169, 739–747. https://doi.org/10.1016/j.petrol.2018.06.029.

Lin, MQ, Zhang, GQ, Hua, Z, Zhao, Q, Sun, FF, 2015. Conformation and plugging properties of crosslinked polymer microspheres for profile control. Colloid. Surface. Physicochem. Eng. Aspect. 477, 49–54. https://doi.org/10.1016/j.colsurfa.2015.03.042.

Lin, MQ, Zhao, Q, Dang, SM, Yang, ZH, Dong, ZX, Zhang, J, 2020. Temperature resistance of AM/AMPS/NVP copolymer microspheres. Iran. Polym. J. (Engl. Ed.) 29, 445–453. https://doi.org/10.1007/s13726-020-00809-5.

Liu, JX, Guo, YJ, Hu, J, Zhang, J, Lv, X, Zhang, XM, et al., 2012. Displacement characters of combination flooding systems consisting of gemini-nonionic mixed surfactant and hydrophobically associating polyacrylamide for bohai offshore oilfield. Energy Fuels 26, 2858–2864. https://doi.org/10.1021/ef3002185.

Liu, YM, Xu, J, Cui, YQ, Liu, LB, Li, JY, 2014. Synthesis, surface properties, and antibacterial activity of quaternary ammonium salts containing epoxide group. J. Dispersion Sci. Technol. 35, 1460–1467. https://doi.org/10.1080/01932691.2013.860878.

Omari, A, Tabary, R, Rousseau, D, Calderon, FL, Monteil, J, Chauveteau, G, 2006. Soft water-soluble microgel dispersions: structure and rheology. J. Colloid Interface Sci. 302, 537–546. https://doi.org/10.1016/j.jcis.2006.07.006.

Pu, J.Y., Geng, J., Han, P., Bai, B.J., 2018a. Preparation and salt-insensitive behavior study of swellable, Cr^{3+}-embedded microgels for water management. J. Mol. Liq. 273, 739–747. https://doi.org/10.1016/j.molliq.2018.10.070.

Pu, W., Zhao, S., Wang, S., Wei, B., Yuan, C., Li, Y., 2018b. Investigation into the migration of polymer microspheres (PMs) in porous media: implications for profile control and oil displacement. Colloid. Surface. Physicochem. Eng. Aspect. 540, 265–275. https://doi.org/10.1016/j.colsurfa.2018.01.018.

Pu, JY, Zhou, J, Chen, YS, Bai, BJ, 2017. Development of thermotransformable controlled hydrogel for enhancing oil recovery. Energy Fuels 31, 13600–13609. https://doi.org/10.1021/acs.energyfuels.7b03202.

Sang, Q, Li, YJ, Yu, L, Li, ZQ, Dong, MZ, 2014. Enhanced oil recovery by branched-preformed particle gel injection in parallel-sandpack models. Fuel 136, 295–306. https://doi.org/10.1016/j.fuel.2014.07.065.

Wang, LZ, Long, YF, Ding, HF, Geng, JM, Bai, BJ, 2017. Mechanically robust Re-crosslinkable polymeric hydrogels for water management of void space conduits containing reservoirs. Chem. Eng. J. 317, 952–960. https://doi.org/10.1016/j.cej.2017.02.140.

Wang, ZY, Lin, MQ, Gu, M, Dong, ZX, Zhang, J, Yang, ZH, 2018. Zr-Induced high temperature resistance of polymer microsphere based on double crosslinked structure. RSC Adv. 8, 19765–19775. https://doi.org/10.1039/C8RA02747A.

Wang, ZY, Lin, MQ, Xiang, YQ, Zeng, TX, Dong, ZX, Zhang, J, Yang, ZH, 2019. Zr-induced thermostable polymeric nanospheres with double-crosslinked architectures for oil recovery. Energy Fuels 33, 10356–10364. https://doi.org/10.1021/acs.energyfuels.9b01463.

Yang, HB, Kang, WL, Zhao, J, Zhang, B, 2015. Energy dissipation behaviors of a dispersed viscoelastic microsphere system. Colloid. Surface. Physicochem. Eng. Aspect. 487, 240–245. https://doi.org/10.1016/j.colsurfa.2015.09.049.

Yang, HB, Kang, WL, Wu, HR, Yu, Y, Zhu, Z, Wang, PX, et al., 2017. Stability, rheological property and oil-displacement mechanism of a dispersed low-elastic microsphere system for enhanced oil recovery. RSC Adv. 7, 8118–8130. https://doi.org/10.1039/C6RA26849H.

Yao, CJ, Lei, GL, Hou, J, Xu, XH, Wang, D, Steenhuis, TS, 2015. Enhanced oil recovery using micron-size polyacrylamide elastic microspheres: underlying mechanisms and displacement experiments. Ind. Eng. Chem. Res. 54, 10925–10934. https://doi.org/10.1021/acs.iecr.5b02717.

Ye, Q, Zhang, ZC, Ge, XW, Ni, YH, Wang, MZ, 2002. Formation of monodisperse poly (methyl methacrylate) particles by radiation-induced dispersion polymerization. II. Particle size and size distribution. Colloid Polym. Sci. 280, 1091–1096. https://doi.org/10.1007/s00396-002-0652-9.

You, Q, Wen, QY, Fang, JC, Guo, M, Zhang, QS, Dai, CL, 2019. Experimental study on lateral flooding for enhanced oil recovery in bottom-water reservoir with high water cut. J. Petrol. Sci. Eng. 174, 747–756. https://doi.org/10.1016/j.petrol.2018.11.053.

Zhao, G, Dai, CL, Gu, CL, You, Q, Sun, YP, 2019. Expandable graphite particles as a novel in-depth steam channeling control agent in heavy oil reservoirs. Chem. Eng. J. 368, 668–677. https://doi.org/10.1016/j.cej.2019.03.028.

Zhao, G, Li, JM, Gu, CL, Li, L, Sun, YP, Dai, CL, 2018. Dispersed particle gel strengthened polymer/surfactant as a novel combination flooding system for enhanced oil recovery. Energy Fuels 32, 11317–11327. https://doi.org/10.1021/acs.energyfuels.8b02720.

Zhao, Q, Lin, MQ, Dang, SM, Hua, Z, 2014. Acrylamide/2-Acrylamido-2-methylpropanesulfonic acid/1-Vinyl-2-pyrrolidinone terpolymeric microspheres by orthogonal experiments. Asian J. Chem. 26, 5615–5618. https://doi.org/10.14233/ajchem.2014.18168.

Zhu, DY, Bai, BJ, Hou, JR, 2017. Polymer gel systems for water management in high-temperature petroleum reservoirs: a chemical review. Energy Fuels 31, 13063–13087. https://doi.org/10.1021/acs.energyfuels.7b02897.

Zhu, DY, Hou, JR, Chen, YG, Zhao, SD, Bai, BJ, 2018. In situ surface decorated polymer microsphere technology for enhanced oil recovery in high-temperature petroleum reservoirs. Energy Fuels 32, 3312–3321. https://doi.org/10.1021/acs.energyfuels.8b00001.